Development and Preliminary Characterization of Ritonavir-Loaded Transethosomal Carriers for Topical Delivery

Siddharth S. Kale[1*], Sucheta D. Bhise[2], Nishant Yalase[1]

[1]PG, Research Scholar Department of Pharmaceutics, Rajgad Dnyanpeeth's College of Pharmacy, Bhor, Pune 412206, Maharashtra, India

[2]Assistant Professor, Department of Pharmaceutics, Rajgad Dnyanpeeth's College of Pharmacy, Bhor, Pune 412206, Maharashtra, India (0009-0002-7535-3233)

Corresponding author

Siddharth S. Kale

Department of Pharmaceutics, Rajgad Dnyanpeeth's College of Pharmacy, Bhor, Pune 412206, Maharashtra, India

E-mail: siddharthkale06@gmail.com (0009-0003-4589-073X)

Abstract

Ritonavir has low aqueous solubility and complex solid-state behaviour, creating substantial formulation challenges. Six ritonavir-loaded transethosomal dispersions (F1-F6) were prepared and compared using analytical, physicochemical, in vitro release and ex vivo skin-permeation parameters. Among the reported batches, F4 showed the smallest particle size (160 nm), the greatest negative zeta-potential magnitude (−36 mV), the highest entrapment efficiency (95%) and drug content (99%), the highest ex vivo flux (25 µg/cm²/h), and 99.2% cumulative release at 360 minutes. Release profiles were examined using zero-order, first-order, Higuchi and Korsmeyer-Peppas equations. Korsmeyer-Peppas produced the highest empirical R^2 values, although mechanistic interpretation is limited by the use of a dialysis-controlled vesicular system. The findings identify F4 as the leading formulation in the available dataset. However, authenticated PDI outputs, replicate-level statistics, complete diffusion-cell documentation, a study-specific ethics approval and experimental stability observations are required before claims of statistical superiority, long-term stability or in vivo performance can be supported.

Keywords: ritonavir; transethosomes; topical delivery; skin permeation; release kinetics; vesicular carriers

How to cite this article: Kale SS, Bhise SD, Yalase N. Development and Preliminary Characterization of Ritonavir-Loaded Transethosomal Carriers for Topical Delivery. Int J Drug Deliv Technol. 2026;16(72s): 445-454. DOI: 10.25258/ijddt.16.72s.55

1. Introduction

Ritonavir is a highly lipophilic HIV protease inhibitor with complex solid-state behaviour. Its conformational polymorphism is a classic example of how crystal form can alter dissolution and product performance, and later studies have confirmed material differences in the physicochemical properties of the polymorphs. [1-3]

Transethosomes combine phospholipid vesicles, ethanol and an edge activator. Ethanol can increase bilayer fluidity and alter stratum-corneum lipid organization, whereas edge activators increase vesicle deformability. Together, these properties can improve the cutaneous transport of poorly soluble compounds, although performance depends strongly on composition, vesicle size, surface charge and the experimental model. [4-9]

A topical or transdermal ritonavir formulation should be regarded as an exploratory drug-delivery platform rather than an established clinical therapy. In vitro release and ex vivo permeation can demonstrate formulation performance, but they do not establish antiviral efficacy, systemic bioavailability or safety. The present study therefore focuses on formulation characterization and comparative performance of six laboratory batches. [10-11]

The study was organized to present the analytical findings first, followed by formulation characterization, in vitro release, ex vivo permeation and stability assessment. The principal objective was to compare six transethosomal batches and identify the composition with the most favourable combined profile, while clearly separating verified experimental observations from information that still requires confirmation.

2. Materials and Methods

2.1 Materials

Ritonavir was received as a gift sample from Flamingo Pharmaceuticals, Navi Mumbai, India. Soybean phosphatidylcholine, phosphatidylethanolamine and the surfactants/edge activators were procured from Vajra Chem Agency, Mumbai, India. Methanol and propylene glycol were obtained from Loba Chemie Pvt. Ltd., India. Purified water was prepared in-house. All reagents were of analytical grade unless otherwise specified.

2.2 Formulation design

Six batches (F1-F6) were prepared with constant quantities of ritonavir, soybean phosphatidylcholine, ethanol and propylene glycol. The edge-activator identity and/or proportion was varied across the batches. The exact edge-activator quantities were not available in the source manuscript and should be copied from the authenticated laboratory batch record before submission.

Component	F1	F2	F3	F4	F5	F6
Ritonavir (mg)	50	50	50	50	50	50
Soybean phosphatidyl choline (mg)	200	200	200	200	200	200
Ethanol (mL)	3	3	3	3	3	3
Propylene glycol (mL)	1	1	1	1	1	1
Edge activator	See batch record	See batch record	See batch record	See batch record	See batch record	See batch record
Purified water	q.s. to 10 mL	q.s. to 10 mL	q.s. to 10 mL	q.s. to 10 mL	q.s. to 10 mL	q.s. to 10 mL

Table 1. Composition stated in the source manuscript. Exact edge-activator amounts require author verification.

Table interpretation: Ritonavir, phospholipid, ethanol and propylene glycol were held constant across F1-F6, so the comparative performance was primarily attributed to the identity and proportion of the edge activator. The exact surfactant quantities must be restored from the authenticated batch record.

2.3 Preparation of transethosomes

Ritonavir, phospholipid and the selected edge activator were dissolved in an ethanol-propylene glycol phase. When sodium deoxycholate was used, it was dissolved in the aqueous phase. The organic phase was evaporated under reduced pressure to form a thin lipid film, which was hydrated with the aqueous phase under controlled agitation. The dispersion was then sonicated or extruded to reduce vesicle size, adjusted to 10 mL with purified water and stored in a tightly closed light-resistant container at 4 degrees C until characterization. The source file did not report evaporation temperature, rotation speed, hydration time, sonication amplitude or duration; these critical process parameters must be inserted from the laboratory record.

2.4 Preformulation studies

2.4.1 UV-visible analysis

Ritonavir solutions were scanned over 200-400 nm to identify the analytical wavelength. Calibration standards of 2-10 µg/mL were prepared in distilled water and pH 6.4 buffer. Absorbance was measured against the corresponding blank, and linear regression of absorbance versus concentration was performed. The method should be supported by validation data for specificity, precision, accuracy, linearity and robustness before use as a stability-indicating assay.

2.4.2 Solubility, melting point and FTIR

Excess ritonavir was equilibrated separately with water, ethanol, methanol, phosphate buffer pH 7.4 and propylene glycol for 24 h at 25 degrees C. Samples were centrifuged, filtered and quantified spectrophotometrically. Melting point was determined by the capillary method. FTIR spectra were recorded over 4000-400 cm-1 and compared with expected functional-group regions to screen for major drug-excipient interactions.

2.4.3 Morphology

The original manuscript included scanning electron micrographs of ritonavir and a formulation sample. The supplied scale bars correspond to the micrometre range and therefore cannot independently verify the nanometre hydrodynamic diameter obtained by DLS. High-magnification SEM or, preferably, transmission electron microscopy should be used for direct vesicle morphology, and the sample preparation, coating, accelerating voltage, magnification and instrument model should be reported.

2.5 Characterization of transethosomal dispersions

2.5.1 Particle size and PDI

The Z-average hydrodynamic diameter and PDI should be determined by dynamic light scattering after suitable dilution with filtered dispersant. Measurements should be made at a defined temperature and scattering angle using at least three independently prepared samples, with the instrument model, viscosity, refractive index and number of runs reported. PDI is required to describe distribution width; a particle-size value without PDI is incomplete. No PDI results were present in the source file.

2.5.2 Zeta potential

Electrophoretic mobility should be measured in a folded capillary cell after controlled dilution, and zeta potential calculated using the instrument-specified model. The dispersant conductivity, pH, measurement temperature and replicate number should be reported. Absolute zeta-potential magnitude is a useful but not sufficient indicator of colloidal stability because steric stabilization and medium composition also contribute.

2.5.3 Entrapment efficiency and drug content

Free drug should be separated from vesicles by a validated ultracentrifugation, ultrafiltration or size-exclusion procedure. Entrapment efficiency should be calculated as EE (%) = [(total drug - free drug)/total drug] x 100. For drug content, vesicles should be disrupted using a suitable solvent and the extracted ritonavir quantified against a validated calibration

curve. Recovery and mass balance should be demonstrated.

2.5.4 pH and viscosity

pH should be measured using a calibrated electrode at 25 degrees C. Viscosity should be measured with a specified Brookfield spindle at a defined rotational speed and temperature. Reporting only one viscosity value without spindle, shear rate and temperature limits reproducibility.

2.6 In vitro drug release and kinetic modelling

Release was studied using a dialysis-membrane method in phosphate buffer pH 7.4 at 37 degrees C. A known amount of formulation should be placed in a pre-equilibrated membrane of stated molecular-weight cut-off, immersed in a defined receptor volume, and agitated at a stated speed. Samples should be withdrawn at predetermined times, replaced with fresh medium and corrected for cumulative dilution. Sink conditions and membrane non-binding should be verified.

The reported mean cumulative-release profiles were fitted by linear regression to zero-order (Qt versus t), first-order [ln(100-Qt) versus t], Higuchi (Qt versus square root of t) and Korsmeyer-Peppas [ln(Mt/Minfinity) versus ln(t)] models. For the Korsmeyer-Peppas model, only observations up to approximately 60% release were used. Model fit was compared using R^2. Because a dialysis-controlled vesicular system is not a classical polymeric matrix, the exponent n was treated as an empirical descriptor rather than definitive proof of a transport mechanism.

2.7 Ex vivo skin permeation

Excised full-thickness abdominal skin from adult Wistar rats was selected as the biological membrane. The skin source, donor characteristics, method of euthanasia, time between excision and testing, and storage conditions should be documented from the authenticated laboratory record. The IAEC certificate supplied separately (IRDI/IAEC/M05/07/2025-26) relates to a different project and investigator and therefore cannot be cited as ethical approval for the present ritonavir study. The correct study-specific IAEC/CPCSEA approval number must be inserted before submission.

Hair should be removed without damaging the stratum corneum, subcutaneous tissue should be trimmed, and skin thickness and storage duration should be documented. Barrier integrity should be confirmed by electrical resistance, transepidermal water loss or an accepted marker before use.

The skin should be mounted in static Franz diffusion cells with the stratum corneum facing the donor compartment. The diffusion area, receptor volume, receptor composition, stirring speed and actual skin-surface temperature should be recorded. The receptor medium must maintain sink conditions for ritonavir. A defined finite dose of formulation should be applied uniformly to the donor surface. Samples should be collected at prespecified times, immediately replaced with fresh medium, filtered and assayed using a validated analytical method.

Cumulative permeated amount per unit area should be plotted against time. Steady-state flux (Jss) is obtained from the slope of the linear region, and the permeability coefficient is calculated as Kp = Jss/C0, where C0 is the drug concentration in the donor formulation. At least six diffusion cells representing skin from multiple donors are recommended. The source manuscript did not report these essential experimental details; therefore, the numerical flux values should be considered preliminary until the laboratory protocol is verified.

2.8 Stability study

A stability protocol should evaluate the optimized formulation in the proposed container-closure system. For an exploratory vesicular dispersion, samples may be stored at 4 +/- 2 degrees C, 25 +/- 2 degrees C and accelerated conditions of 40 +/- 2 degrees C/75 +/- 5% RH, with testing at 0, 1, 2, 3 and 6 months. Formal product-development studies should follow applicable ICH expectations and use stability-indicating analytical procedures. Attributes should include appearance, phase separation, pH, particle size, PDI, zeta potential, drug content, entrapment efficiency, degradation products and release profile.

Condition	Time points	Tests	Proposed acceptance criteria
4 ± 2°C	0, 1, 2, 3 and 6 months	Appearance, pH, particle size, PDI, zeta potential, entrapment efficiency, assay and release profile	All results must comply with the parameter-specific criteria below
25 ± 2°C/60 ± 5% RH	0, 1, 2, 3 and 6 months	Appearance, pH, particle size, PDI, zeta potential, entrapment efficiency, assay and release profile	All results must comply with the parameter-specific criteria below
40 ± 2°C/75 ± 5% RH	0, 1, 2, 3 and 6 months	Appearance, pH, particle size, PDI, zeta potential, entrapment efficiency, assay, release profile and degradation products	All results must comply with the parameter-specific criteria below

Table 2. Recommended stability-study framework. No stability results were present in the source manuscript.

Table interpretation: The framework distinguishes refrigerated, long-term and accelerated storage conditions and requires monitoring of both physical and chemical stability. Acceptance criteria should be predefined from validated methods and actual development data rather than inferred from literature alone.

2.9 Statistical analysis

Each experiment should be conducted using at least three independent formulation preparations, and each reported result should be expressed as mean +/- standard deviation with the exact n stated. Single-endpoint comparisons among F1-F6 should be performed using one-way ANOVA followed by Tukey multiple-comparison testing after checking normality and homogeneity of variance. Release and permeation profiles should be compared using an appropriate repeated-measures or mixed-effects model, with formulation and time as factors. A two-sided P value below 0.05 may be considered statistically significant. The source dataset lacked replicate-level observations; therefore, SD values, ANOVA and P values could not be calculated validly and no claims of statistical significance are made in this revision.

3. Results

3.1 UV calibration

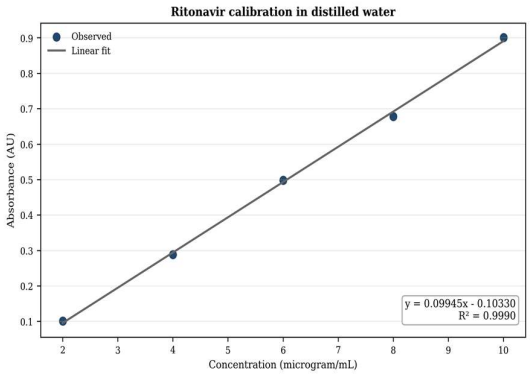

Figure 1. Calibration curve of ritonavir in distilled water.

Interpretation: Absorbance increased linearly across 2-10 µg/mL, and the reported R^2 of 0.9990 indicates strong proportionality within the tested range. This result supports routine quantification, although accuracy, precision, specificity and robustness still require formal validation.

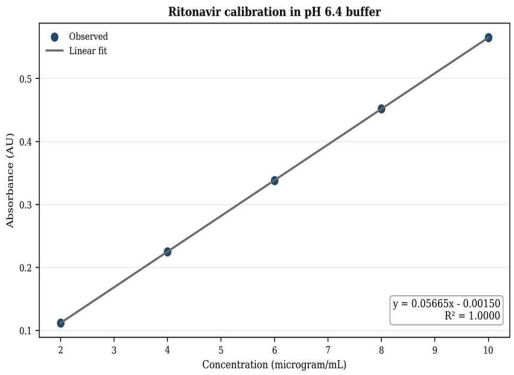

Figure 2. Calibration curve of ritonavir in pH 6.4 buffer.

Interpretation: The buffer calibration produced an essentially linear response (R^2 = 1.0000) over the reported concentration range. The lower slope relative to distilled water indicates a medium-dependent analytical response and supports the use of matrix-matched calibration standards.

The distilled-water calibration showed the regression equation y = 0.09945x - 0.10330 with R^2 = 0.9990. The pH 6.4 buffer calibration showed y = 0.05665x - 0.00150 with R^2 = 1.0000 over the reported 2-10 µg/mL range. High linearity alone does not constitute full analytical-method validation; precision, accuracy, selectivity and robustness remain to be documented.

3.2 Solubility, melting point and FTIR

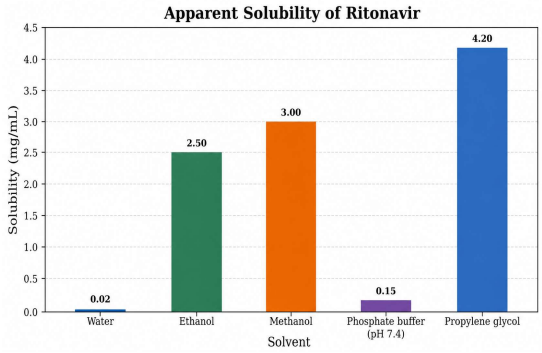

Figure 3. Apparent solubility of ritonavir in selected solvents.

Interpretation: Ritonavir displayed marked solvent dependence. Propylene glycol produced the highest apparent solubility, followed by methanol and ethanol, whereas water and phosphate buffer showed limited solubilization. The pattern supports the inclusion of co-solvents in the transethosomal system.

Ritonavir showed the lowest reported solubility in water (0.02 mg/mL) and the highest in propylene glycol (4.2 mg/mL). Ethanol and methanol also increased apparent solubility relative to aqueous media. These findings support the use of a co-solvent-rich vesicular system but should be confirmed using a validated, equilibrium solubility method with replicate values.

The observed melting points (123-124 degrees C) were within the range stated in the source manuscript. Because ritonavir is polymorphic, melting point alone is insufficient for solid-form identification; DSC and powder X-ray diffraction are recommended for confirmation. [1-3]

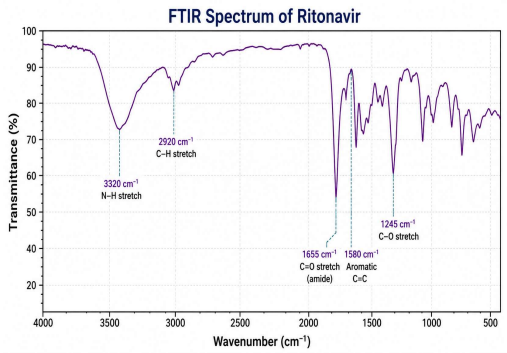

Figure 4. FTIR spectrum of ritonavir with the principal reported absorption bands.

Interpretation: The bands assigned to N-H, amide C=O, aromatic C=C, C-O and aliphatic C-H vibrations remained within their expected spectral regions. The result is consistent with retention of the principal ritonavir functional groups, but it does not by itself exclude subtle drug-excipient interactions.

Functional group	Observed peak (cm-1)	Expected region (cm-1)
N-H stretch	3320	3300-3400
C=O stretch (amide)	1655	1640-1660
Aromatic C=C	1580	1570-1600
C-O stretch	1245	1230-1250
C-H stretch	2920	2900-2950

Table 3. Key FTIR peaks reported in the source manuscript.

Table interpretation: Every listed peak falls within the corresponding expected region, supporting the identity of the principal functional groups. Compatibility should nevertheless be evaluated using complete overlaid spectra and documented peak-shift or intensity analysis.

The key peaks remained within their expected regions, with no major shift reported. This qualitative comparison suggests the absence of a gross chemical incompatibility, but full spectra, peak-intensity changes and replicate measurements are required for a robust compatibility conclusion.

3.3 Morphology

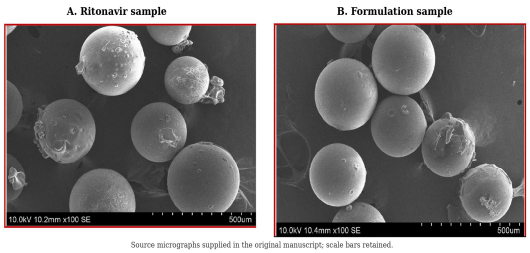

Figure 5. SEM micrographs supplied for ritonavir and the formulation sample.

Interpretation: The micrographs show rounded structures and differences in surface texture; however, their micrometre-scale bars do not permit direct confirmation of the nanometre hydrodynamic diameters measured by DLS. TEM or higher-resolution electron microscopy is required for vesicle-scale confirmation.

The supplied micrographs show rounded structures and surface heterogeneity. However, the scale bars are in the micrometre range, and the images do not resolve 160-280 nm vesicles. The morphology claim should therefore be limited to the visual features shown. A higher-resolution TEM or SEM dataset is required to corroborate nanovesicle size and lamellarity.

3.4 Particle size, PDI and zeta potential

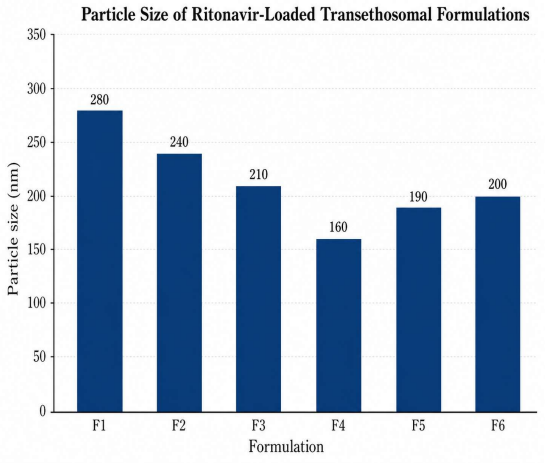

Figure 6. Particle size of formulations F1-F6.

Interpretation: Particle size decreased from F1 to F4 and then increased modestly in F5 and F6. F4 showed the smallest reported diameter (160 nm), suggesting that its composition produced the greatest size reduction among the six batches.

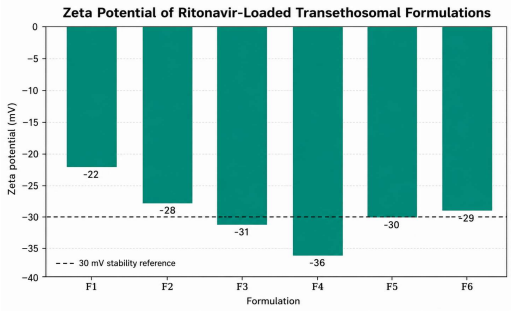

Figure 7. Zeta potential of formulations F1-F6.

Interpretation: F4 exhibited the greatest negative surface-potential magnitude (−36 mV). F3 and F5 were close to −30 mV, whereas F1 had the lowest magnitude. These values provide a descriptive indication of electrostatic stabilization but must be considered together with PDI, medium composition and storage behaviour.

Batch	Particle size (nm)	PDI	Zeta potential (mV)	Replicate reporting
F1	280	Not available	−22	Not reported
F2	240	Not available	−28	Not reported
F3	210	Not available	−31	Not reported
F4	160	Not available	−36	Not reported
F5	190	Not available	−30	Not reported
F6	200	Not available	−29	Not reported

Table 4. Reported DLS and zeta-potential data. PDI and replicate-level outputs were not available in the supplied dataset.

Table interpretation: F4 had the smallest reported particle size and the greatest negative zeta-potential magnitude. Because PDI and replicate measurements were unavailable, the uniformity and statistical reproducibility of the formulations cannot be established from this table.

F4 had the smallest reported Z-average diameter (160 nm) and the greatest negative zeta-potential magnitude (-36 mV). These values identify F4 as the most promising batch in the source dataset. Nevertheless, selection based on particle size is incomplete without PDI, correlogram quality and replicate variability. The manuscript therefore does not describe F4 as statistically smaller or definitively more homogeneous.

3.5 Entrapment efficiency, drug content, pH and viscosity

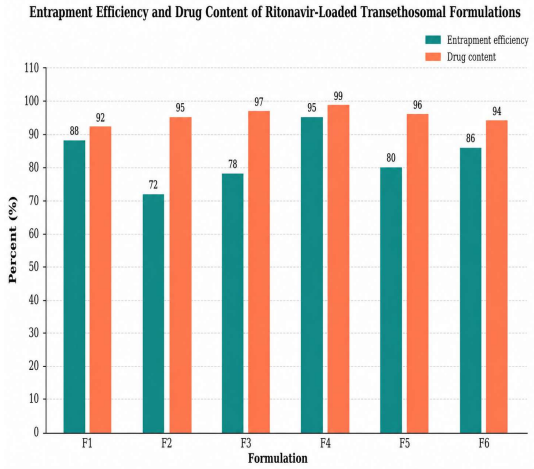

Figure 8. Entrapment efficiency and drug content of formulations F1-F6.

Interpretation: F4 combined the highest reported entrapment efficiency (95%) with the highest drug content (99%). The comparatively low entrapment of F2 suggests that the edge-activator composition strongly influenced drug retention within the vesicles.

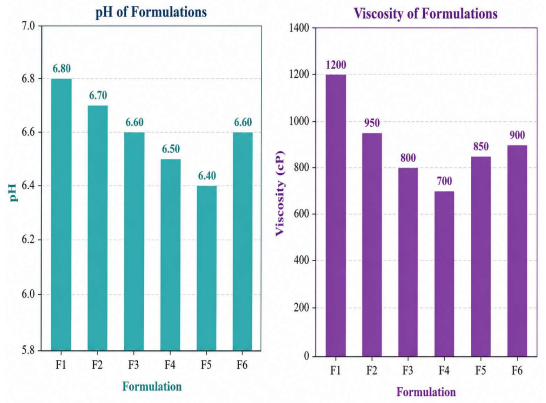

Figure 9. pH and viscosity of formulations F1-F6.

Interpretation: All batches were within the reported pH range of 6.4-6.8. F4 had the lowest viscosity (700 cP), which may favour spreading and diffusion, whereas F1 showed the highest viscosity and may offer greater residence but lower ease of application.

Batch	EE (%)	Drug content (%)	pH	Viscosity (cP)
F1	88	92	6.8	1200
F2	72	95	6.7	950
F3	78	97	6.6	800
F4	95	99	6.5	700
F5	80	96	6.4	850
F6	86	94	6.6	900

Table 5. Values transcribed from the source manuscript; SD and n were not available.

Table interpretation: F4 showed the most favourable combined profile for entrapment, drug content and

viscosity, while its pH remained within the range reported for the other batches. These are descriptive comparisons and require replicate measurements for formal statistical evaluation.

F4 showed the highest reported entrapment efficiency (95%) and drug content (99%), together with a pH of 6.5 and the lowest reported viscosity (700 cP). The pH range of 6.4-6.8 is broadly compatible with topical use, but skin compatibility must be established experimentally. The viscosity data require instrument settings and replicate variability before comparative rheological conclusions can be accepted.

3.6 In vitro drug release and kinetic modelling

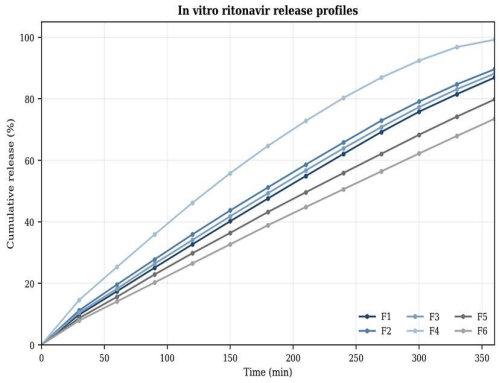

Figure 10. Cumulative in vitro release of ritonavir from formulations F1-F6.

Interpretation: All formulations showed progressive release over 360 minutes. F4 released ritonavir most rapidly and reached 99.2%, while F6 showed the slowest profile and reached 73.5%. The differences indicate a strong influence of vesicle composition on drug partitioning and membrane-mediated release.

Time (min)	F1	F2	F3	F4	F5	F6
0	0.0	0.0	0.0	0.0	0.0	0.0
30	9.8	11.2	10.5	14.6	8.7	7.9
60	17.4	19.6	18.2	25.3	15.6	14.1
90	25.1	27.8	26.4	35.9	22.9	20.3
120	32.7	35.9	34.1	46.2	29.8	26.5
150	40.2	43.7	41.8	55.8	36.4	32.7
180	47.6	51.2	49.3	64.7	43.2	38.9
210	54.9	58.6	56.7	72.8	49.6	44.8
240	62.1	65.8	63.9	80.3	55.9	50.6
270	69.2	72.9	70.8	86.9	62.1	56.4
300	75.8	79.1	77.3	92.4	68.3	62.2
330	81.5	84.7	83.1	96.8	74.2	67.9
360	86.9	89.6	88.2	99.2	79.8	73.5

Table 6. Cumulative in vitro release (%) reported for formulations F1-F6.

Table interpretation: F4 remained the highest-releasing batch at every sampled interval. F1-F3 formed an intermediate group, whereas F5 and F6 released more slowly, demonstrating that formulation composition altered both the rate and extent of drug release.

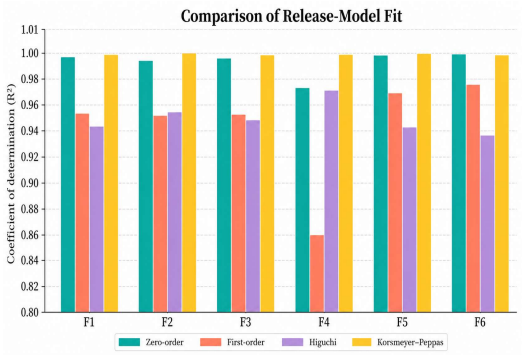

Figure 11. Comparison of coefficients of determination for the fitted release models.

Interpretation: The Korsmeyer-Peppas model gave the highest R^2 for every formulation, while zero-order fitting was also strong for most batches. These comparisons describe the mathematical shape of the profiles; they should not be treated as definitive proof of a single molecular transport mechanism.

Batch	k0	R^2 zero	k1	R^2 first	kH	R^2 Higuchi	n (K-P)	R^2 K-P
F1	0.24166	0.9972	0.00053	0.9541	4.9739	0.94036	0.8898	0.9994
F2	0.24778	0.9939	0.00059	0.9526	5.1381	0.95040	0.8544	0.9996
F3	0.24447	0.9959	0.00056	0.9533	5.0541	0.94083	0.8728	0.9991
F4	0.27771	0.9740	0.01133	0.8592	5.8562	0.97016	0.8355	0.9995
F5	0.21988	0.9981	0.00422	0.9695	4.5195	0.94023	0.9012	0.9997
F6	0.20188	0.9991	0.00335	0.9763	4.1368	0.93072	0.9022	0.9994

Table 7. Release-kinetic parameters calculated from the reported mean profiles. K-P, Korsmeyer-Peppas.

Table interpretation: Korsmeyer-Peppas R^2 values were uniformly high, and the empirical exponent ranged from 0.8355 to 0.9022. Because the test used a dialysis-controlled vesicular dispersion rather than a classical polymer matrix, the exponent is best reported as a comparative descriptor.

F4 reached 99.2% reported release at 360 min, whereas F6 reached 73.5%. The Korsmeyer-Peppas model produced the highest R^2 values for all formulations (0.9991-0.9997), and the zero-order model also fitted F1-F3, F5 and F6 closely (R^2 0.9939-0.9991). The calculated n values ranged from 0.8355 to 0.9022. These values describe the empirical shape of the early release curves; they should not be used alone to assign a polymer-matrix mechanism to transethosomal dispersions.

3.7 Ex vivo skin permeation

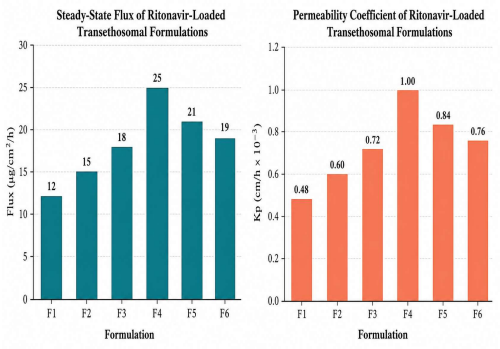

Figure 12. Ex vivo skin-permeation flux and permeability coefficient of formulations F1-F6.

Interpretation: F4 produced the highest reported flux and permeability coefficient, followed by F5 and F6. This ranking is consistent with the smaller vesicle size and higher drug loading of F4, although biological replication and statistical analysis are needed before superiority can be established.

Batch	Flux (µg/cm²/h)	Kp (cm/h × 10^{-3})
F1	12	0.48
F2	15	0.60
F3	18	0.72
F4	25	1.00
F5	21	0.84
F6	19	0.76

Table 8. Ex vivo permeation values reported in the available dataset; donor number, diffusion-cell replication, SD and inferential statistics were not available.

Table interpretation: The flux and permeability coefficient followed the same batch ranking, with F4 highest and F1 lowest. The apparent advantage of F4 should be confirmed using multiple skin donors, at least six diffusion cells where feasible, verified sink conditions and a validated assay.

The reported flux increased from 12 µg/cm²/h for F1 to 25 µg/cm²/h for F4, with corresponding Kp values of 0.48 × 10^{-3} and 1.00 × 10^{-3} cm/h. F4 therefore had the highest descriptive permeation value. Because the source file omitted skin source, donor number, diffusion area, receptor composition, sink verification, SD and P values, the results cannot be described as statistically superior and should be confirmed under the detailed protocol in Section 2.7.

3.8 In vivo study status

No in vivo pharmacokinetic, antiviral-efficacy, dermal-irritation or systemic-safety experiment was included in the available study record. Accordingly, the present work reports analytical characterization, in vitro release and ex vivo skin permeation only. Any statement regarding in vivo bioavailability, therapeutic efficacy or clinical performance should be deferred until an appropriately approved animal study is completed and reported.

3.9 Stability assessment

No authenticated time-dependent stability observations were supplied for the optimized formulation. Therefore, numerical values for particle size, PDI, zeta potential, pH, entrapment efficiency, assay, degradation products and release at 1, 2, 3 or 6 months are not presented as experimental findings. The protocol in Table 2 should be completed using measurements generated from the final container-closure system before any shelf-life or long-term-stability claim is made.

4. Discussion

Across the available analytical and formulation data, F4 showed the most favourable overall profile. Its smaller reported diameter, greater negative zeta-potential magnitude, high entrapment efficiency and high drug content were accompanied by the fastest in vitro release and the greatest descriptive ex vivo flux. This coordinated pattern is consistent with the recognized influence of edge-activator composition, ethanol content and vesicle deformability on transethosomal performance.

The release behaviour of F4 may reflect enhanced ritonavir solubilization, increased bilayer fluidity, a shorter diffusion path and rapid partitioning into the receptor medium. Although the Korsmeyer-Peppas equation produced the highest R^2 values, dialysis-membrane resistance and drug partitioning can contribute substantially to the observed profile. Consequently, the fitted exponent should be treated as an empirical comparison rather than conclusive evidence of a polymer-matrix transport mechanism.

The most important analytical limitation is the absence of authenticated replicate-level observations. A single mean particle-size value cannot describe distribution width, and statistical comparisons cannot be reconstructed without independent batches and raw measurements. Instrument reports should be used to restore PDI, correlogram quality, measurement settings, replicate number and variability before submission.

The ex vivo permeation results also require complete experimental documentation. Skin donor information, anatomical site, integrity testing, diffusion area, receptor composition, sink verification, temperature, applied dose, sample-replacement correction and biological replication all influence the calculated flux. The supplied ethical certificate pertains to another project and cannot serve as approval for this study; the correct study-specific IAEC/CPCSEA documentation must be provided.

5. Limitations

- The formulation batch record did not provide exact edge-activator quantities or complete process parameters.
- Most reported results were single summary values; SD, n, ANOVA and P values could not be reconstructed.

- PDI and DLS quality outputs were absent.
- The study-specific ethics approval and several essential Franz-cell parameters were not verified; the separately supplied certificate belongs to another project.
- Stability observations and degradation-product data were absent.
- The study did not include antiviral activity, dermal irritation, pharmacokinetics or in vivo efficacy; therefore, clinical effectiveness and bioavailability cannot be claimed.

6. Conclusion

The comparative dataset identifies F4 as the leading ritonavir-loaded transethosomal formulation because it combined the smallest reported particle size with the greatest negative zeta-potential magnitude, the highest entrapment efficiency and drug content, the highest descriptive ex vivo flux and nearly complete release at 360 minutes. The study supports further development of F4 as a topical vesicular carrier, but the evidence remains preliminary. Before journal submission, the authors should provide authenticated PDI and replicate data, complete analytical validation and Franz-cell parameters, the correct study-specific ethics approval, and experimental stability observations. No conclusion regarding in vivo efficacy, systemic bioavailability or clinical performance should be made from the present data.

Data Availability

The numerical summary data used in this revision were transcribed from the supplied manuscript. Replicate-level raw data, DLS/PDI instrument files, Franz-cell worksheets and stability datasets were not supplied. The corresponding author should archive and make these source records available according to the target journal policy.

Acknowledgments

The authors thank Rajgad Dnyanpeeth's College of Pharmacy, Bhor, Pune, for providing facilities for the research work.

Conflict of Interest

The authors declare no conflict of interest.

Financial Support and Sponsorship

Nil.

Author Contributions

Siddharth S. Kale performed the experimental work and prepared the initial manuscript. Sucheta D. Bhise supervised the research, contributed to data interpretation and reviewed the manuscript. Nishant Yalase contributed to the study as stated by the authors; the specific CRediT role should be confirmed before submission.

References

1. Bauer J, Spanton S, Henry R, Quick J, Dziki W, Porter W, et al. Ritonavir: an extraordinary example of conformational polymorphism. Pharm Res. 2001;18(6):859-866.
2. Wang C, Rosbottom I, Turner TD, Laing S, Maloney AGP, Sheikh AY, et al. Molecular, solid-state and surface structures of the conformational polymorphic forms of ritonavir in relation to their physicochemical properties. Pharm Res. 2021;38:971-990.
3. Rodriguez-Spong B, Acciacca A, Fleisher D, Rodriguez-Hornedo N. pH-induced nanosegregation of ritonavir to lyotropic liquid crystal of higher solubility than crystalline polymorphs. Mol Pharm. 2008;5(6):956-967.
4. Abdulbaqi IM, Darwis Y, Khan NAK, Abou Assi R, Khan AA. Ethosomal nanocarriers: the impact of constituents and formulation techniques on ethosomal properties, in vivo studies, and clinical trials. Int J Nanomedicine. 2016;11:2279-2304.
5. Raj A, Dua K, Nair RS, Chandran CS, Alex AT. Transethosome: an ultra-deformable ethanolic vesicle for enhanced transdermal drug delivery. Chem Phys Lipids. 2023;255:105315.
6. Seenivasan R, Halagali P, Nayak D, Tippavajhala VK. Transethosomes: a comprehensive review of ultra-deformable vesicular systems for enhanced transdermal drug delivery. AAPS PharmSciTech. 2025;26(1):41.
7. El Zaafarany GM, Awad GA, Holayel SM, Mortada ND. Role of edge activators and surface charge in developing ultradeformable vesicles with enhanced skin delivery. Int J Pharm. 2010;397(1-2):164-172.
8. Albash R, Abdelbary AA, Refai H, El-Nabarawi MA. Use of transethosomes for enhancing the transdermal delivery of olmesartan medoxomil: in vitro, ex vivo, and in vivo evaluation. Int J Nanomedicine. 2019;14:1953-1968.
9. Bin Jardan YA, Ahad A, Raish M, Al-Jenoobi FI. Preparation and characterization of transethosome formulation for the enhanced delivery of sinapic acid. Pharmaceutics. 2023;15(10):2391.
10. Faria MJ, Machado R, Ribeiro A, Goncalves H, Real Oliveira MECD, Viseu T, et al. Rational development of liposomal hydrogels: a strategy for topical vaginal antiretroviral drug delivery in the context of HIV prevention. Pharmaceutics. 2019;11(9):485.
11. Trommer H, Neubert RHH. Overcoming the stratum corneum: the modulation of skin penetration. Skin Pharmacol Physiol. 2006;19(2):106-121.
12. Fissan H, Ristig S, Kaminski H, Asbach C, Epple M. Comparison of different characterization methods for nanoparticle dispersions before and after aerosolization. Anal Methods. 2014;6:7324-7334.

13. Higuchi T. Mechanism of sustained-action medication: theoretical analysis of rate of release of solid drugs dispersed in solid matrices. J Pharm Sci. 1963;52(12):1145-1149.
14. Korsmeyer RW, Gurny R, Doelker E, Buri P, Peppas NA. Mechanisms of solute release from porous hydrophilic polymers. Int J Pharm. 1983;15(1):25-35.
15. Siepmann J, Peppas NA. Higuchi equation: derivation, applications, use and misuse. Int J Pharm. 2011;418(1):6-12.
16. Ng SF, Rouse J, Sanderson D, Eccleston G. Validation of a static Franz diffusion cell system for in vitro permeation studies. AAPS PharmSciTech. 2010;11(3):1432-1441.
17. Neupane R, Boddu SHS, Renukuntla J, Babu RJ, Tiwari AK. Alternatives to biological skin in permeation studies: current trends and possibilities. Pharmaceutics. 2020;12(2):152.
18. Oh L, Shah VP, Curtis J, et al. In vitro skin permeation methodology for over-the-counter topical dermatologic drug products. AAPS J. 2020;22:120.
19. International Council for Harmonisation. ICH Q1A(R2): Stability testing of new drug substances and products. Geneva: ICH; 2003.